Available online at www.sciencedirect.com
ScienceDirect
Applied Catalysis B: Environmental 80 (2008) 1–14
APPLIED CATALYSIS B: ENVIRONMENTAL
www.elsevier.com/locate/apcatb

Influence of the acidity of nanostructured CoMo/P/Ti-HMS catalysts on the HDS of 4,6-DMDBT reaction pathways

B. Pawelec [a], J.L.G. Fierro [a], A. Montesinos [b], T.A. Zepeda [a,b,*]

[a] *Instituto de Catálisis y Petroleoquímica, CSIC, Cantoblanco, E-28049 Madrid, Spain*[1]
[b] *Centro de Ciencias de la Materia Condensada, UNAM, CP. 22800 Ensenada, B.C., Mexico*[2]

Received 28 August 2007; received in revised form 24 October 2007; accepted 27 October 2007
Available online 12 November 2007

Abstract

The influence of catalyst acidity on the reaction mechanism of the 4,6-dimethyldibenzothiophene (4,6-DMDBT) hydrodesulfurization (HDS) over CoMo hydrotreating catalysts was studied using a batch autoclave and fixed-bed reactor (T = 598 K and P = 5.5 MPa). P-free Ti-HMS and P-containing P/Ti-HMS mesoporous siliceous materials were synthesized and used as supports. The effect of the catalyst preparation method (successive vs. simultaneous impregnation) and phosphorous addition on catalyst acidity was studied by TPD-NH_3 and DRIFT-NH_3 techniques. For all synthesized catalysts, the reaction proceeds *via* dealkylation (DA) and isomerization (ISO) pathways, with the later being the main reaction route. Incorporation of Co and Mo phases by simultaneous impregnation was found to be the best method for catalyst preparation, whereas P-addition promote the isomerization route of 4,6-DMDBT transformation to a greater extent than the dealkylation route. On the contrary, the reaction on a CoMoP/γ-Al_2O_3 reference catalyst proceeds *via* HYD and DDS reaction pathways, the later being the main reaction route. The catalyst acidity–activity correlation indicates that both activity and selectivity depend largely on the presence of Brønsted acid sites as well as on the total amount of Brønsted and Lewis acid sites. By correlating HRTEM-activity data, the enhancement of activity and isomerization observed with the catalyst prepared by simultaneous impregnation and modified with P was related to the cumulative effects of the lower size of MoS_2 slabs and their higher surface density.

Keywords: HDS; DBT; 4,6-DMDBT; CoMo catalysts; Mesoporous silica; Phosphorous; Brønsted acidity

1. Introduction

The removal of sulfur from heavy diesel fractions is receiving increasing interest due to new environmental legislation requiring the further reduction of sulfur content. In 2009, the sulfur content from diesel fractions needs to be lower than 10 ppm [1]. In order to meet these specifications, there is a need for more efficient processes and more active catalysts. Traditional hydrodesulfurization (HDS) catalysts are Mo or W supported on alumina promoted by Ni or Co in sulfided state [2–5]. However, these catalysts are unable to achieve the deep HDS of alkyl-substituted dibenzothiophenes (DBT). Thus, new effective HDS catalysts are based on the totally different concept of bulk-like materials. For example, the unsupported NEBULA catalysts developed jointly by Akzo Nobel, Nippon Ketjen and Exxon Mobil and commercialized in 2001 are effective for deep HDS [6]. However, this new generation of catalysts is more expensive than the supported ones. Thus, the challenge is to design novel cost-effective supported catalysts.

The difficulty in converting alkyl-substituted DBTs over classical Co(Ni)-Mo/γ-Al_2O_3 catalysts is commonly ascribed to the steric hindrance of the alkyl groups, especially when both are in the 4- and 6-positions, which hinder the adequate interaction of the S-atom with the catalytic active site. Thus, the challenge is to engineer new catalysts (metals as well as supports) which can eliminate the planar configuration of alkyl-substituted DBT. Such destruction of the planar configuration of those compounds could be achieved through the hydrogenation of their aromatic rings, dealkylation, isomerization or C–C bond scission reactions [7–10].

* Corresponding author at: Centro de Ciencias de la Materia Condensada, UNAM, CP. 22800 Ensenada, B.C., Mexico. Tel.: +52 6461744602x353; fax: +52 6461744603.
E-mail address: trino@icp.csic.es (T.A. Zepeda).
[1] http://www.icp.csic.es/eac/index.htm.
[2] http://www.ccmc.unam.mx/investiga/cat/menu_i_cat.html.

0926-3373/$ – see front matter © 2007 Elsevier B.V. All rights reserved.
doi:10.1016/j.apcatb.2007.10.039

In order to promote the migration of methyl groups in the aromatic ring structure, attempts were made to change the acid properties of support by use of the hybrid materials, e.g. HY-Al_2O_3 [10,11], HY-SiO_2 [11,12], ZSM-5/Al_2O_3 [10], SiO_2–Al_2O_3 [12] or Al_2O_3–TiO_2 [13]. In this sense, the higher hydrogenation/hydrogenolysis ratio was reported by Robinson et al. [7] for the HDS of 4E6MDBT over CoMo catalysts supported on Al_2O_3–SiO_2. The activity enhancement over the acid support was ascribed to the C–C bond scission in the thiophenic ring either before or after the desulphurization step [8]. For the HDS of 4,6-DMDBT, the effect of Al_2O_3-support modification by HY addition on the activity of CoMo catalysts was reported by Landau et al. [10] and Isoda et al. [11]. It was found that steric hindrance was diminished by the migration of methyl groups in the aromatic ring, but the reactants were cracked simultaneously due to the acidic nature of the catalysts [10,11]. For CoMo/Al_2O_3 catalysts tested in the HDS of 4,6-DMDBT, the effect of the modification of alumina acidity by P-loading was studied by Kwak et al. [14]. They found that the P_2O_5 content in the catalyst up to 0.5 wt% enhances catalytic activity due to the modification of molybdenum dispersion and Brønsted acidity by acid treatment. The authors proposed that an increase in Brønsted acidity allows the migration of the methyl groups in 4,6-DMDBT, thereby reducing steric hindrance in the adsorption of this compound on the catalyst surface [14]. Manoli et al. [15] observed that the addition of P increased both the number of Lewis sites and Mo^{4+} abundance in P-doped monometallic Mo carbide catalysts supported on alumina. Thus, a linear correlation was found between the intensity of the band at 1608 cm^{-1} (from pyridine IR spectra), which is characteristic of coordination sites, and Mo^{4+} abundance derived from XPS analysis.

The influence of the catalyst preparation conditions on the surface of P-modified alumina-supported Mo catalysts has been studied by several authors [16–19]. In general, it was found that the co-impregnation was superior method of the catalyst preparation with respect to sequential impregnation [16–19]. However, in the case of Mo impregnation preceding Co impregnation, the better performance in HDS reaction was also reported [20]. Similarly to alumina-supported catalysts modified with P [14,15], our recent study on the CoMoP/HMS catalysts demonstrated that the morphology of the sulfided CoMo species depends on the method of catalyst preparation and on the P-concentration on the surface of HMS support, with the former factor being more important than the later [21]. The successive impregnation catalysts were less active in the HDS reaction of DBT than that prepared by simultaneous impregnation. We attributed the higher catalytic activity of the latter samples to the larger surface exposure of both Co and Mo sulfided species [21]. On the other hand, our previous study showed that Ti-loading into hexagonal mesoporous silica (HMS) material has a positive effect on the activity of supported CoMo catalysts in the HDS of DBT and 4E6MDBT [22]. Regarding this later reaction, we observed that after Ti-incorporation into HMS material, additional acid-catalyzed isomerization occurs. With respect to a conventional CoMoP/Al_2O_3 sample, the CoMo/Ti-HMS catalyst with Si/Ti = 40 showed greater selectivity toward isomerization route products.

Within the above scope, this work was undertaken to study the influence of both catalyst preparation method (successive vs. simultaneous impregnation) and catalyst acidity on the reaction mechanism of 4,6-DMDBT hydrodesulphurization over CoMo catalysts performed using a batch and fixed-bed reactors. The catalysts were supported on HMS modified by both Ti and P (P/Ti-HMS). The synthesized bare supports and CoMo catalysts were characterized by N_2 adsorption–desorption isotherms (S_{BET}), X-ray diffraction (XRD), X-ray photoelectron spectroscopy (XPS), high-resolution transmission electron microscopy (HRTEM), temperature-programmed desorption (TPD) of NH_3, and DRIFTS of adsorbed NH_3 in order to correlate catalytic activity with catalyst structure.

2. Experimental

2.1. Synthesis of the pure supports and catalysts

The Ti-HMS material (Si/Ti molar ratio of 40) was prepared following a procedure similar to that described by Gotier and Tuel [23] using dodecylamine ($C_{12}H_{25}NH_2$, Aldrich 98%) as surfactant. The procedure followed during preparation has been described elsewhere [22,24]. The P-containing material (P/Ti-HMS) was prepared by impregnation of the calcined Ti-HMS material (pore filling method) with the required amount of H_3PO_4 (Fluka; 85 wt% in water). The material obtained was dried at room temperature for 16 h and then at 378 K for 2 h, and finally calcined in air at 773 K for 4.5 h, reaching this temperature in 3.5 h. The zero point charges (ZPC) of the Ti-HMS and P/Ti-HMS materials were 5.1 and 4.8, respectively.

The P-free and P-containing CoMo catalysts were prepared by successive (SUC) and simultaneous (SIM) impregnations using the pore filling method. The catalysts will be labeled hereafter as SUC, SUC-P, SIM and SIM-P. Regarding the successive impregnation method, the catalyst preparation procedure involved the first impregnation with aqueous solution of $(NH_4)_6Mo_7O_{24}{\cdot}4H_2O$ (Aldrich 99%; pH 4). Thereafter the solid was dried at room temperature for 18 h and then at 378 K for 2 h. After this, the calcination was performed at 773 K for 4.5 h, reaching this temperature within 3.5 h. Then the second impregnation was performed with an aqueous solution of $Co(NO_3)_2{\cdot}6H_2O$ (Aldrich 98%; pH 8) followed by drying and calcination as before was carried out. In the catalysts prepared by simultaneous impregnation method (SIM, SIM-P), the cobalt and molybdenum were added from an aqueous solution of $(NH_4)_6Mo_7O_{24}{\cdot}4H_2O$ (Aldrich 99%) and $Co(NO_3)_2{\cdot}6H_2O$ (Aldrich 98%; pH 8). The solid was dried at room temperature for 18 h and then at 378 K for 2 h. Finally, calcination was performed at 773 K for 4.5 h, reaching this temperature within 3.5 h. All supported CoMo catalysts on the Ti-HMS material were prepared with nominal composition of 3.0 and 9.0 wt% of Co and Mo, respectively (Co/(Co + Mo) atomic ratio = 0.32). Both P-containing catalysts show nominal P content of 0.64 wt%.

2.2. Characterization methods

The textural properties of the naked supports and calcined catalysts were determined by N_2 adsorption–desorption isotherms at 77 K with ASAP 2000 Micromeritics equipment. Prior to the experiments, all samples were degassed at 543 K in a vacuum for 5 h. The volume of adsorbed N_2 was normalized to standard temperature and pressure. Pore size distribution (PSD) of the naked supports was evaluated by applying the Barret–Joyner–Halenda method (BJH) to the adsorption branch of the N_2 isotherm. Specific surface area (S_{BET}) was calculated by the BET equation applied to the range of relative pressures $0.05 < P/P^0 < 0.30$. The normalized BET area was calculated according to the following equation:

$$\text{normalized}, S_{BET} = \frac{S_{BET\ of\ catalyst}}{(1-y) \times S_{BET\ of\ support}} \quad (1)$$

where y is the weight fraction of the guest phases.

The zero point charge determination of the synthetized supports was determined by mass titration. In short, in this method the variation of pH of a water solution containing increasing amount of solid was monitored until the steady-state values of pH (ZPC) was reached.

The X-ray patterns were recorded on a Rigaku 2100 diffractometer, using monochromatic Cu Kα radiation ($\lambda = 0.1541$ nm). The diffractograms were recorded in the 2θ range of 0.15–80° at a step of 0.02°.

For the high magnification TEM study, the sulfided (10% H_2S in H_2, 673 K) catalysts were ultrasonically dispersed in *i*-octane at room temperature and then spread out on a holey carbon–copper microgrid. TEM images were collected on a JEOL TEM-3000F microscope operating at 300 kV. The average lengths and stacking of the MoS_2 particles were estimated from 450 nanoparticles taken from 12 images.

The acidity of the naked supports and oxide catalysts was determined by TPD-NH_3 measurements using an Altamira TPD/TPR device. The calcined samples (0.05 g) were first degassed in a He flow (Air Liquide, 99.996%) at 483 K for 1 h. Then, the samples were saturated with a mixture of 10% NH_3/He stream at 373 K for 25 min. The physically adsorbed NH_3 was then removed by treatment in a He flow for 30 min at 353 K. The ammonia desorption was performed from 353 to 1050 K using a He flow and heating rate of 15 K min^{-1}, while recording TCD signal. The DRIFT spectra of adsorbed NH_3 were acquired with a Nicolet 510 FTIR spectrophotometer, using a Harrick HVCDRP cell that allows *in situ* treatments with different gases at temperatures up to 773 K. The interferograms were obtained after 500 scans using a KBr spectrum as background. About 30 mg of finely ground sample was placed in a sample holder and pretreated *in situ* in the DRIFT cell. The samples were cooled under a flow of He and then treated with NH_3 (900 ppm NH_3–He) at 305 K and ambient pressure by passing a NH_3/He mixture through the cell for 30 min.

The amount of coke deposited on the catalysts was determined using thermogravimetric TGA/SDTA851 equipment (Mettler Toledo), measuring the weight losses upon oxidation of coked catalysts. The burning of coke was carried out by raising the sample temperature to a final temperature of 1073 K at a rate of 10 K min^{-1} in a 20% O_2/N_2 mixture.

X-ray photoelectron spectra of the sulfided and used catalysts were recorded using a VG Escalab 200R spectrometer equipped with a hemispherical electron analyzer and a Mg Kα ($h\nu = 1253.6$ eV) X-ray source. In order to protect the samples from the contact with air, they were kept in *i*-octane until being transferred into the XPS apparatus. The samples were first placed in a copper holder mounted on a sample-rod in the pretreatment chamber of the spectrometer and then degassed at 420 K for 1 h before transfer to the analysis chamber. All catalysts were degassed at 10^{-5} mbar and then transferred to the ion-pumped analysis chamber, where residual pressure was kept below 7×10^{-9} mbar during data acquisition. The binding energies (BE) were referenced to the C 1s peak (284.9 eV) to account for the charging effects. Analyses of the peaks were performed with the software provided by VG and using non-linear least squares fitting program. The mixed 90%Gaussian/10%Lorentzian functions were employed after background subtraction according to Shirley. Surface atomic ratios were calculated from the peak area ratios normalized by the corresponding atomic sensitivity factors provided with the software.

2.3. Catalytic activity measurements

2.3.1. HDS reaction performed in a batch reactor

The sulfided catalysts were tested in a HDS reaction of 4,6-DMDBT performed in a batch Parr reactor charged with 0.2 g of the catalyst and 0.3 g of 4,6-DMDBT dissolved in 100 ml of decalin. In order to minimize internal diffusion limitations, all catalysts were thoroughly ground to a fine powder. The reaction conditions were: $T = 598$ K, $P = 5.5$ MPa and 1000 rpm. The reactor took 35 min to reach the reaction temperature. Before the catalytic test, the reactor was purged with nitrogen to remove traces of oxygen. The absence of internal/external diffusion limitations was confirmed by varying the amount of catalyst and the power of stirring (1000, 800 and 700 tpm). The reaction products were analyzed by GC on a PerkinElmer XL device using a 30 m long Altech-Econo capillary column. The mass balance in all experiments was within the 99.80–99.98% range. The kinetic rate constants were used as a measure of catalytic activity. HDS kinetic rate constants were calculated assuming pseudo-first order kinetics referred to 4,6-DMDBT concentration according to the following equation:

$$k = \frac{-\ln(1-x)}{t} \quad (2)$$

where x is 4,6-DMDBT concentration and t is reaction time.

2.3.2. HDS reaction performed in a fixed-bed reactor

The HDS of 4,6-DMDBT (dissolved in decalin) was performed in a high-pressure laboratory-scale set-up equipped with a stainless steel fixed-bed catalytic reactor. A 0.25 g of the catalyst with particles of a sieve fraction of 0.25–0.3 mm was diluted with 5 g of SiC. The 4,6-DMDBT flow was 4.69×10^{-5} $mol_{(4,6\text{-DMDBT})}$ min^{-1}. The liquid mixture was

injected (0.25 ml min^{-1}) by a high-pressure pump (HPLC Knauer) into a hydrogen stream (60 ml min^{-1}). The reaction was carried out at 598 K and 5.5 MPa of total pressure employing H_2 flow rate of 7 L(STP) h^{-1}. Weight hour space velocity (WHSV) was kept at 46.4 h^{-1}. Before catalyst activation, the catalyst was dried under a N_2 flow of 100 ml min^{-1} at 423 K for 0.5 h. The catalyst was then sulfided *in situ* at atmospheric pressure by a mixture of 10 vol% of a H_2S:H_2 at a rate of 60 ml min^{-1} for 4 h at 673 K (isothermal). After sulfidation, the catalyst was purged under a N_2 flow of 100 ml min^{-1} at 473 K for 0.5 h, and it was left overnight under a N_2 flow of 3 ml min^{-1}. Before the experimental runs, the N_2 pressure was increased to the desired value, and the catalytic bed was heated to the reaction temperature. After the experimental run, the reactor effluents were condensed, and liquid samples were periodically collected and analyzed by gas–liquid chromatography (Varian chromatograph Model Star 3400 CX) using a flame ionization detector (FID) and a 30 m × 0.53 mm DB^{-1} column (100% methylpolysiloxane, J&W Scientific) as a stationary phase. For all experimental runs, the conversion was kept low enough in order to differential reactor conditions to be ensured. The specific reaction rates were calculated according to the following equation:

$$\nu(\mathrm{mol}_{(4,6\text{-DMDBT})}\,\mathrm{mmol}_{(\mathrm{Me})}^{-1}\,\mathrm{s}^{-1}) = \frac{\mathrm{mol}_{(4,6\text{-DMDBT})}/\mathrm{s}}{\mathrm{mmol}_{(\mathrm{Me})}} X_{(4,6\text{-DMDBT})} \quad (3)$$

where Me is equal to total metal content (mmol Mo + mmol Co). For comparison purposes, the activity of a commercial $CoMoP/Al_2O_3$ catalyst (AKZO KF-752; S_{BET} = 223 $m^2\,g^{-1}$; pore diameter = 6.6 nm; 14.2 wt% Mo; 3.8 wt% Co; 0.83 wt% P) was also measured. This catalyst was developed by Akzo Nobel in the 1992–1993 timeframe for HDS of diesel feed [25].

3. Results and discussion

3.1. Textural properties of the supports and catalysts

The textural properties of the naked supports and oxide catalysts were evaluated from N_2 sorption data obtained at 77 K. The specific surface area (S_{BET}), total pore volume (V_p) and average pore diameter are compiled in Table 1. The P-free support (Ti-HMS) shows slightly higher BET area value (961 $m^2\,g^{-1}$) than the P-containing P/Ti-HMS support (932 $m^2\,g^{-1}$). The pore size distributions of both naked materials are shown in Fig. 1. Both materials show the same pore size distributions (PSD) with the pore sizes in the range of 1–6 nm. The average pore diameter is somewhat larger in the P-free support than in the P-containing material (3.4 nm vs. 3.3 nm). This is likely due to the presence of deposited phosphates on the P/Ti-HMS support surface. The low-angle XRD data (not shown here) excluded the formation of segregated P_2O_5 species.

As expected, the S_{BET} specific area value of the support decreases after deposition of Mo and Co components followed by calcination (Table 1). The larger decrease in both S_{BET} specific area and pore volume values is observed in samples prepared by successive impregnation. It is noteworthy that all synthesized catalysts show a high specific surface area (634–793 $m^2\,g^{-1}$) after calcination, with both P-free catalysts showing a larger specific surface area than their P-containing counterparts. Considering average pore diameter, one might note that both catalysts prepared by simultaneous impregnation have a larger one than their counterparts prepared by successive impregnation (3.6 nm vs. 3.4 nm). The decrease in pore diameter could be indicative of the location of Co and Mo species within the pores of substrate [26]. In order to clarify this point, the normalized surface areas (NS_{BET}) of the oxide catalysts were calculated according to Eq. (1). The values of the NS_{BET} are compiled in Table 1. Both SUC and SUC-P samples show lower NS_{BET} than their SIM and SIM-P counterparts (0.78 vs. 0.89–0.99) indicating location of part of the metal oxide species within the pores of the substrate when successive impregnation is employed. It is noteworthy that, contrary to the catalysts prepared by simultaneous impregnation, both SUC and SUC-P samples show the same average pore diameter (3.4 nm) and normalized surface areas (ca. 0.78) indicating the location of P species on the external surface of SUC-P sample. To conclude, simultaneous impregnation led to better textural properties of the CoMo catalysts (larger S_{BET} and pore diameter) than successive impregnation. For the former catalysts, the metal oxide species are located exclusively on the support surface whereas for the latter samples the bimodal metal oxides distribution on the support surface and within the pores was achieved. For all catalysts, the metal oxides are located mainly on the external support surface.

Table 1
Textural properties[a] of the oxide catalysts and HRTEM data of the sulfided catalysts

Samples	Labeling	S_{BET} (NS_{BET}) (m^2/g_{cat})	Pore diameter (nm)	Pore volume (cm^3/g)	Particle size (nm)	Stacking spacing (nm)	Surface density of MoS_2 particles ($MoS_{2(particles)}$/50 nm^2)
Ti-HMS	Ti-HMS	961	3.4	1.74	–	–	–
P/Ti-HMS	P/Ti-HMS	932	3.3	1.72	–	–	–
Co/Mo/Ti-HMS[b]	SUC	655 (0.78)	3.4	0.99	4.4 ± 0.09	0.597 ± 0.01	1.9 ± 0.2
Co/Mo/P/Ti-HMS[b]	SUC-P	634 (0.79)	3.4	1.02	4.0 ± 0.08	0.599 ± 0.01	2.6 ± 0.2
CoMo/Ti-HMS[c]	SIM	743 (0.89)	3.6	1.16	3.7 ± 0.03	0.605 ± 0.01	3.3 ± 0.1
CoMo/P/Ti-HMS[c]	SIM-P	793 (0.99)	3.6	1.27	3.3 ± 0.06	0.611 ± 0.01	4.2 ± 0.3

[a] As determined by N_2 sorption isotherms at 77 K. Normalized surface area values (NS_{BET}; Eq. (1)) are given in parentheses.
[b] Prepared by successive impregnation using the pore filling method.
[c] Prepared by simultaneous impregnation using the pore filling method.

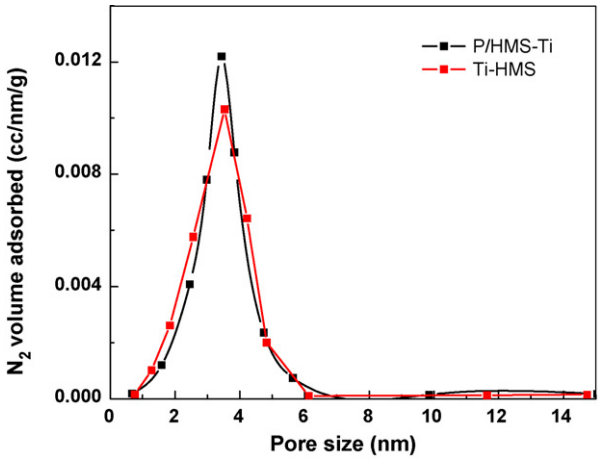

Fig. 1. Pore size distribution of the naked Ti-HMS and P/Ti-HMS materials.

3.2. Characterization of the sulfided catalysts

XRD measurements were used to study the crystalline phases of the samples after sulfidation. The X-ray patterns of the pure Ti-HMS and P/Ti-HMS supports and sulfided catalysts, prepared by both successive and simultaneous impregnation, in the interval from 5° to 80° 2θ are shown in Fig. 2(a) and 2(b), respectively. The X-ray patterns of all samples show a broad line between 20° and 30°, which is attributed to the amorphous part of the substrates [27]. No reflections belonging to both Mo and Co phases were observed.

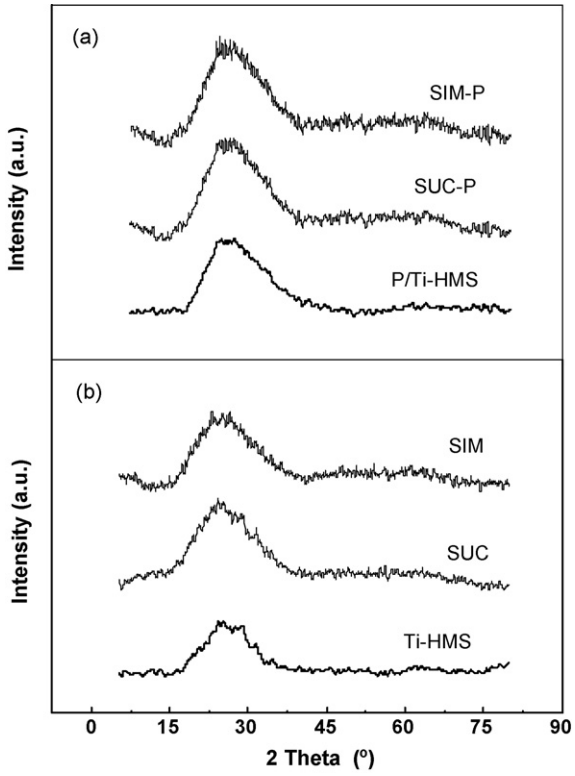

Fig. 2. Wide-angle X-ray diffraction patterns of the sulfided CoMo/Ti-HMS and CoMo/P/Ti-HMS catalysts prepared by successive (a) and simultaneous (b) impregnation methods.

Irrespective of the catalyst preparation method and P-content, the samples showed high dispersion of the supported Co and Mo species.

The effect of catalyst preparation and P-incorporation on the stacking of MoS_2 slabs in the sulfided samples was evaluated by HRTEM. The high-resolution electron microscopy images of the sulfided samples are displayed in Fig. 3. The total sulfidation of the Mo atoms was confirmed by XPS of the sulfided samples discussed below. For all samples, typical MoS_2 slabs randomly distributed on the support can be identified from their typical fringes with a stacking spacing of between 0.58 and 0.63 nm (spacing characteristic to pure MoS_2 phase). HRTEM parameters such as crystal size and surface density of MoS_2 particles are compiled in Table 1. As seen in this table, MoS_2 particle size decreases in the following order: SUC > SUC-P > SIM > SIM-P, whereas the surface density of MoS_2 particles follows the reverse trend. Particle size was very low for all catalysts (in the range 3.3–4.4 nm) and the surface density of MoS_2 particles per 50 nm^2 was in the range of 1.9–4.2. The samples prepared by SIM procedure show particles with larger stacking spacing (0.61 nm) than their counterparts prepared by SUC one (0.6 nm). Although it was found that P-incorporation increases the stacking spacing of the MoS_2 (Table 1), this could be due to the complex interactions between MoS_2 and support. Thus, the effect of P is not clear and further experiments are needed to explain the influence of P ions on the expansion of the MoS_2 layers.

3.3. Catalyst acidity

TPD-NH_3 profiles were obtained in order to compare the acidity of oxide catalysts and naked supports. The TPD-NH_3 profiles and the Gaussian deconvolution lines of representative samples (SUC-P and SIM-P) are shown in Fig. 4. The peaks corresponding to weak ($T < 550$ K), medium (550 K < $T < 750$ K) and strong ($T > 750$ K) acid sites were obtained. The concentrations of the weak, medium and strong strength acid sites, expressed as mmoles of NH_3 desorbed, are collected in Table 2. TPD-NH_3 data of the reference CoMoP/γ-Al_2O_3 sample are included in this table (profiles not shown here). One can note that the naked supports show weak, medium and strong strength acid sites with the main contribution of weak and medium strength acid sites. The SUC and SUC-P catalysts show only the presence of weak and strong strength acid sites (Table 2), while the SIM and SIM-P samples show medium strength acid sites. The total acidity of the samples was calculated as the sum of the weak, medium and strong strength acid sites obtained after fitting of the experimental curves to sum of Gaussian lines (Table 2). All catalysts showed higher total acidity than their homologous supports and the SIM-P sample showed the largest total acidity among the catalysts studied. The total acidity of the samples follows the trend: SIM-P > SIM ≈ SUC-P > SUC ≫ commercial CoMoP/γ-Al_2O_3. All samples show larger total acidity in comparison to the commercial one. Considering our previous study on the effect of Ti incorporation into the CoMo/HMS systems [22], this is linked with the presence of Ti species. Additionally, the presence of a phosphate phase on the surface

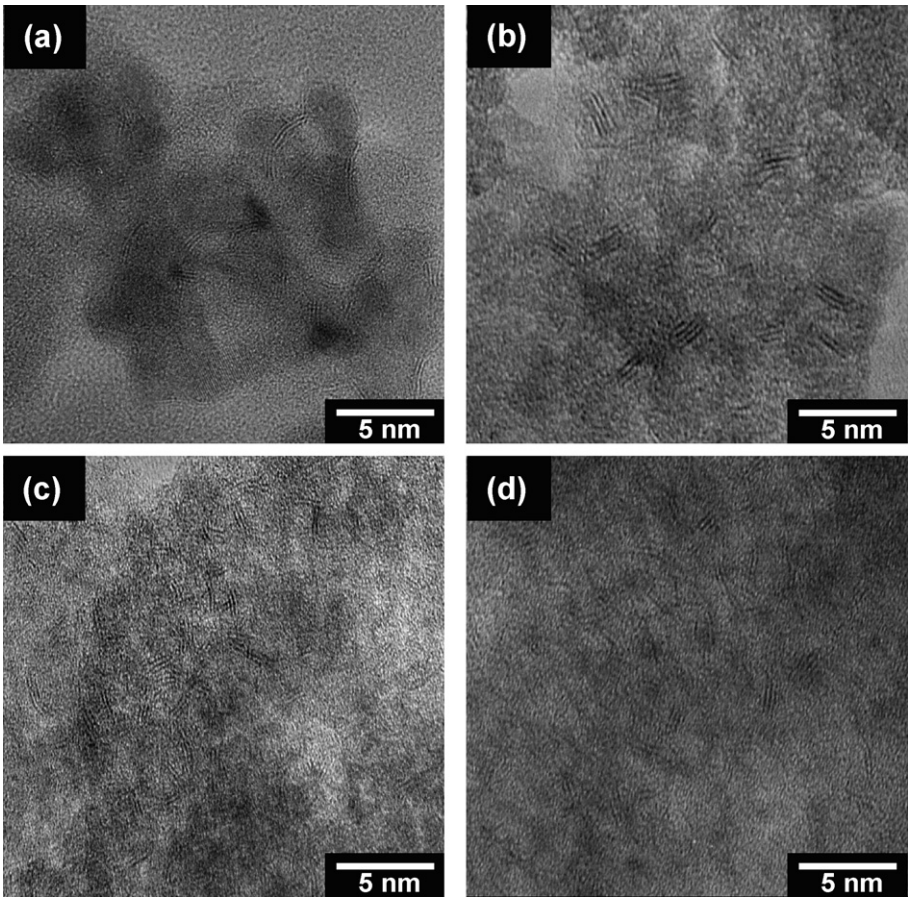

Fig. 3. HRTEM images of the sulfided catalysts prepared by successive or simultaneous impregnation methods: SUC (a), SUC-P (b), SIM (c) and SIM-P (d).

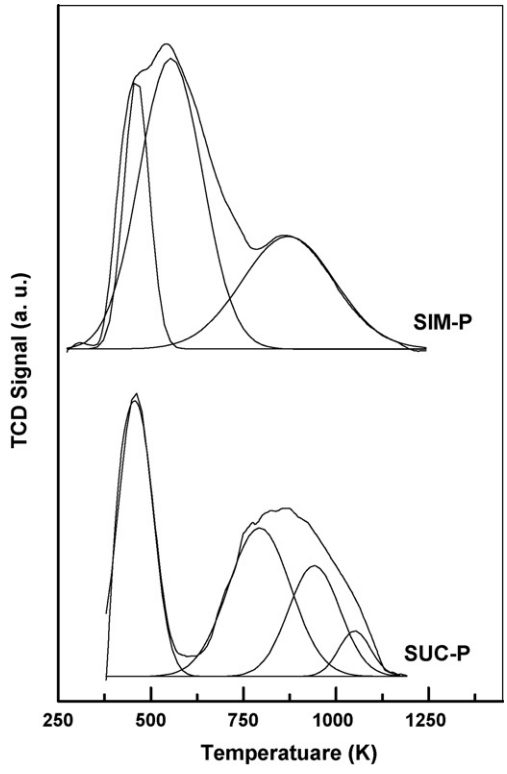

Fig. 4. TPD-NH_3 profiles and the Gaussian deconvolution lines of the calcined samples.

of the Ti-HMS material led to the formation of weak acid sites. Interestingly, the commercial CoMoP/γ-Al_2O_3 sample show lower amount of weak and strong strength acid sites than the other samples (Table 2).

In order to distinguish the type of acid sites, DRIFT spectra of adsorbed ammonia were recorded. Fig. 5 shows the DRIFT spectra of adsorbed ammonia on the oxide catalysts and naked Ti-HMS and P/Ti-HMS supports. After NH_3 adsorption at room temperature, the pure Ti-HMS and P/Ti-HMS supports showed a minor band at ca. 1653 cm^{-1} and a main absorption band ca. 1578 cm^{-1}, while the spectra of all catalysts showed bands at ca. 1653, 1578, 1380 and 1275 cm^{-1}. The SUC sample shows an additional absorption band at 1486 cm^{-1}. The bands at 1653 and 1486 cm^{-1} come from the symmetric and asymmetric vibration of NH_4^+ ions adsorbed on Brønsted acid sites on the surface (δ_{sym}(H-N-H)) [28–30]. The band at 1578 cm^{-1} is ascribed to the deformation modes of coordinated NH_3 species adsorbed over Lewis acid sites on the catalyst, which is commonly assigned to δ_{asym}(H-N-H), whereas the band at 1275 cm^{-1} is characteristic of δ_{sym}(H-N-H) over Lewis acid sites [31]. Finally, the band at 1380 cm^{-1} is due to the adsorption of NH_3 species over Brønsted acid surface sites [31].

Table 2 shows the ranking of acid sites considering the DRIFT spectra of NH_3 adsorbed on the Brønsted (B) and Lewis (L) sites. The commercial CoMoP/γ-Al_2O_3 sample (spectra not reported) did not record Brønsted acidity at all and the amount

Table 2
Acidity of the oxide CoMo/P/Ti-HMS catalysts

Sample	Strength of acid sites[a] (mmol NH_3 g_{cat}^{-1})			Total	Type acid sites[b] (relative area)		
	Weak (<500 K)	Medium (500–650 K)	Strong (>650 K)		Brønsted (B)	Lewis (L)	B/L ratio
Ti-HMS	0.26	0.10	0.06	0.42	0.03	0.32	0.09
P/Ti-HMS	0.21	0.18	0.10	0.49	0.05	0.36	0.14
SUC	0.11	–	0.63	0.74	0.33	0.56	0.60
SUC-P	0.30	–	0.59	0.89	0.48	0.57	0.84
SIM	0.18	0.38	0.30	0.86	0.41	0.55	0.74
SIM-P	0.28	0.59	0.32	1.19	0.59	0.40	1.48
CoMoP/γ-Al_2O_3	0.05	0.36	0.08	0.49	0.04	0.49	0.08

[a] Calculated from amount of desorbed NH_3 by TPD profiles.
[b] Area of the Gaussian deconvolution bands (from DRIFT-NH_3 spectra).

of Lewis acid sites is the lowest among the catalysts studied, as derived from the area of the corresponding bands (Table 2). As seen in Table 2, the SIM-P catalyst shows the largest Brønsted acidity and the lowest Lewis acidity among the catalysts studied. More information could be obtained by analyzing the Brønsted-to-Lewis acidity ratio (B/L ratio). The B/L ratio follows the order: SIM-P (1.48) > SUC-P (0.84) > SIM (0.74) > SUC (0.60) > reference CoMoP/Al_2O_3 (0.08). Comparing the B/L ratio values of catalysts with their homologous support one can note an increase in the amount of Brønsted acid sites linked with the presence of Co and Mo ions on the Ti-HMS surface. A larger acidity of the naked Ti-HMS and P/Ti-HMS supports with respect to the reference catalyst is also observed (Table 2). Regardless of the impregnation method, both P-containing catalysts (SUC-P and SIM-P) show the largest concentration of Brønsted acid sites, indicating that P-addition might change the electronic properties of the catalyst surface.

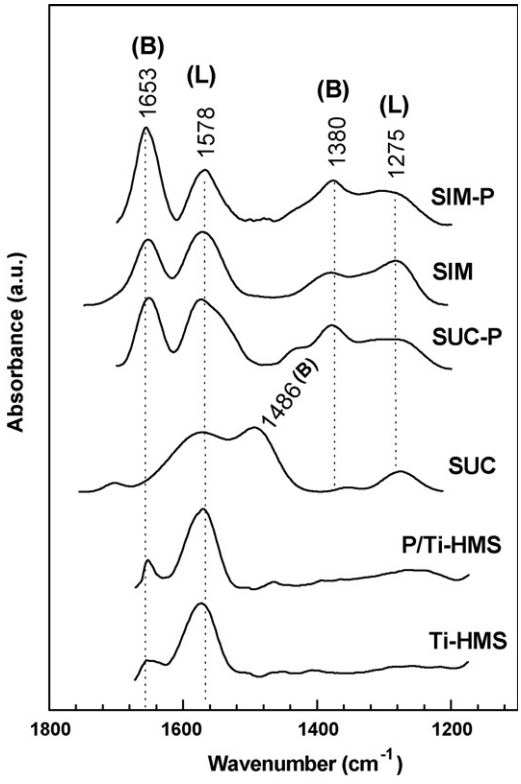

Fig. 5. DRIFTS spectra of NH_3 adsorbed at room temperature of the calcined samples.

3.4. Catalytic activity measurements

3.4.1. Catalytic test performed in a batch reactor

It is known that S-containing compounds such as 4,6-DMDBT are much more refractory for desulphurization than the DBT molecule. This is linked to the presence of methyl groups located at the 4 and 6 positions of DBT, which inhibit S-atom adsorption on the active site. Thus, both catalysts series (SUC and SIM) were tested in the HDS of 4,6-DMDBT (batch reactor, $T = 598$ K, total pressure of 5.5 MPa). A commercial CoMoP/γ-Al_2O_3 catalyst was used as reference.

Fig. 6(a) compares the pseudo-first order rate constants k after 6 h of reaction time calculated according to Eq. (1) and expressed as mol of 4,6-DMDBT per mol of metal-content (Co + Mo) and per second. As seen in this figure, the catalysts prepared by SIM show a higher HDS activity with respect to their counterparts prepared by SUC impregnation. Irrespective of the preparation method employed, P-addition to Ti-HMS support enhances catalyst activity. Thus, the SIM-P catalyst records the highest activity among the catalysts studied in this reaction, including the industrial one. This sample is 2.5 times more active than its P-free counterpart (SIM sample) and 9 times more active than the reference sample.

More information on the effects of P and the preparation method could be obtained by analyzing the product distribution in Table 3, calculated at the same conversion of ca. 50%. From this table, it is clear that the commercial catalyst shows the traditional HDS of 4,6-DMDBT reaction pathways: DDS (3,3′-dimethyl-biphenyl) and HYD (3-(3′-methylcyclohexyl)toluene) as shown in Scheme 1(a). On the other hand, the HDS of 4,6-DMDBT over all synthesized catalysts occurs *via* dealkylation, which led to DBT formation, and *via* isomerization (main route) as indicated in Scheme 1(b). Thus, all the catalysts studied here show higher isomerization activity to facilitate desulfurization of molecules such as 4,6-DMDBT. Considering the isomerization route, one may note that 3,6-DMDBT was not detected by GC analysis. Thus, one may infer that the reactivity of this intermediate product is very high and it is rapidly transformed

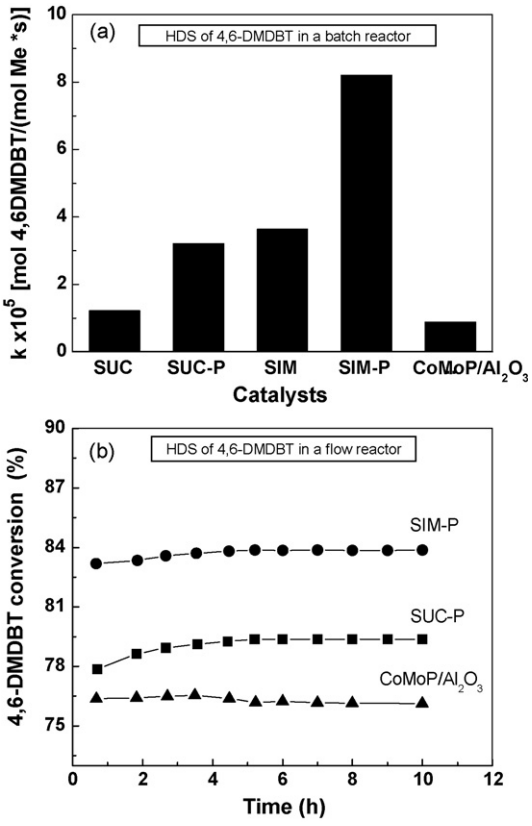

Fig. 6. HDS of 4,6-DMDBT. (a) Pseudo first-order reaction rate constant (batch reactor; $t = 6$ h). (b) 4,6-DMDBT conversion vs. time on-stream (flow reactor).

into 3,4′-dimethyl-biphenyl (3,4′-DMBP) and 3-(4′-methylcyclohexyl)toluene (3,4′-MCTH) products.

In order to evaluate the influence of P, as well as the effect of the preparation method on product distribution, the ISO/DA and HYD/DDS ratios were calculated at similar 4,6-DMDBT conversion (ca. 50%). By analyzing ISO/DA ratios compiled in Table 3, it is clear that both the presence of P and SIM impregnation had a positive effect on the isomerization route of this reaction, with the effect of the P-addition being more pronounced. On the other hand, the balance of hydrolysis and hydrogenation functionalities is also an important requirement for designing effective hydrotreating catalysts. In this connection, the HYD/DDS ratio represents selectivity for hydrogenation functionality versus selectivity toward products of the DDS reaction route. Comparing the HYD/DDS ratio of the catalysts compiled in Table 3, it is noted that for all catalysts, including the commercial one, this ratio is close to 1, indicating the equal contribution of both reaction routes to total activity in the target reaction. Moreover, it appears that the presence of P on the HMS support, as well as the use of simultaneous impregnation, did not lead to an increase in the hydrogenation functionality of the catalysts.

3.4.2. Catalytic test performed in a flow-reactor

It is known that in the case of the HDS 4,6-DMDBT reaction performed in a batch reactor, the inhibition of the reaction due to the accumulation of intermediate products and H_2S in the batch reactor might occur [22]. Thus, the two P-containing catalysts prepared in this study by SUC and SIM impregnation were also studied in the HDS of 4,6-DMDBT reaction performed a flow fixed-bed reactor at 598 K and 5.5 MPa total pressure. Again, the reference catalyst was a commercial CoMoP/γ-Al_2O_3 sample. Product distribution and the specific reaction rates calculated using Eq. (2) and 4,6-DMDBT conversion data taken at time on-stream (TOS) of 0 and 10 h (steady-state conditions) are given in Table 4. As seen in this table, in close agreement with a catalytic test performed in a batch reactor, both SUC-P and SIM-P samples showed higher catalytic activity in comparison to the reference sample, and the SIM-P sample recorded a higher catalytic activity (5.8%) than the SUC-P. These results are quite interesting considering that the reference catalyst has a considerably higher metal content (14 wt% Mo and 3.8 wt% Co) than the SUC-P and SIM-P samples (9 wt% Mo and 3 wt% Co). This means that future optimization of metal loading is possible.

Irrespectively of the reactor used for the activity test, the commercial CoMoP/γ-Al_2O_3 sample displays the classical HDS reaction pathway of 4,6-DMDBT: DDS and HYD, as the main products over this sample were 3,3′-dimethyl-biphenyl (3,3′-DMBP) and 3-(3′-methylcyclohexyl)toluene (3,3′-MCHT), respectively (see Scheme 1(a)). Contrary to the

Table 3
Conversion and products distribution data for the HDS of 4,6-DMDBT over synthesized catalysts and reference sample

Catalyst	Products distribution (%)[a]							Selectivity ISO/DA[b] ratio	Selectivity HYD/DDS[c] ratio	4,6-DMDBT conv. (%)
	DBT	THDBT	BP	CHB	DCH	3,4′-DMBP	3,4′-MCHT			
SUC	7.5	4.2	6.9	2.9	2.9	13.8	11.8	1.04	1.05	56.2
SUC-P	6.1	3.8	4.6	2.1	2.2	16.7	14.5	1.65	1.06	69.1
SIM	4.2	2.1	8.1	4.3	2.2	16	13.1	1.39	0.90	61.3
SIM-P	2.8	4.3	3.9	2.4	1.2	18.8	16.6	2.42	1.08	92.2

Catalyst	Products distribution (%)[a]							Selectivity ISO/DA[b] ratio	Selectivity HYD/DDS[c] ratio	4,6-DMDBT conv. (%)
	DBT	THDBT	BP	CHB	DCH	3,3′-DMBP	3,3′-MCHT			
CoMoP/γ-Al_2O_3	0.0	0.0	0.0	0.0	0.0	24.3	25.7	–	1.1	59.0

[a] At ca. 50% of 4,6-DMDBT conversion.
[b] Dealkylation (DA) route vs. isomerization (ISO) route products: [(DBT + THDBT + BP + CHB + DCH)/(3,4′-DMBP + 3,4′-MCHT)].
[c] Hydrogenation route (HYD) vs. direct desulfurization (DDS) route products: [(3,4′-MCHT (or 3,3′-MCHT) + THDBT + CHB + DCH)/(3,4′-DMBP (or 3,3′-DMBP) + BP].

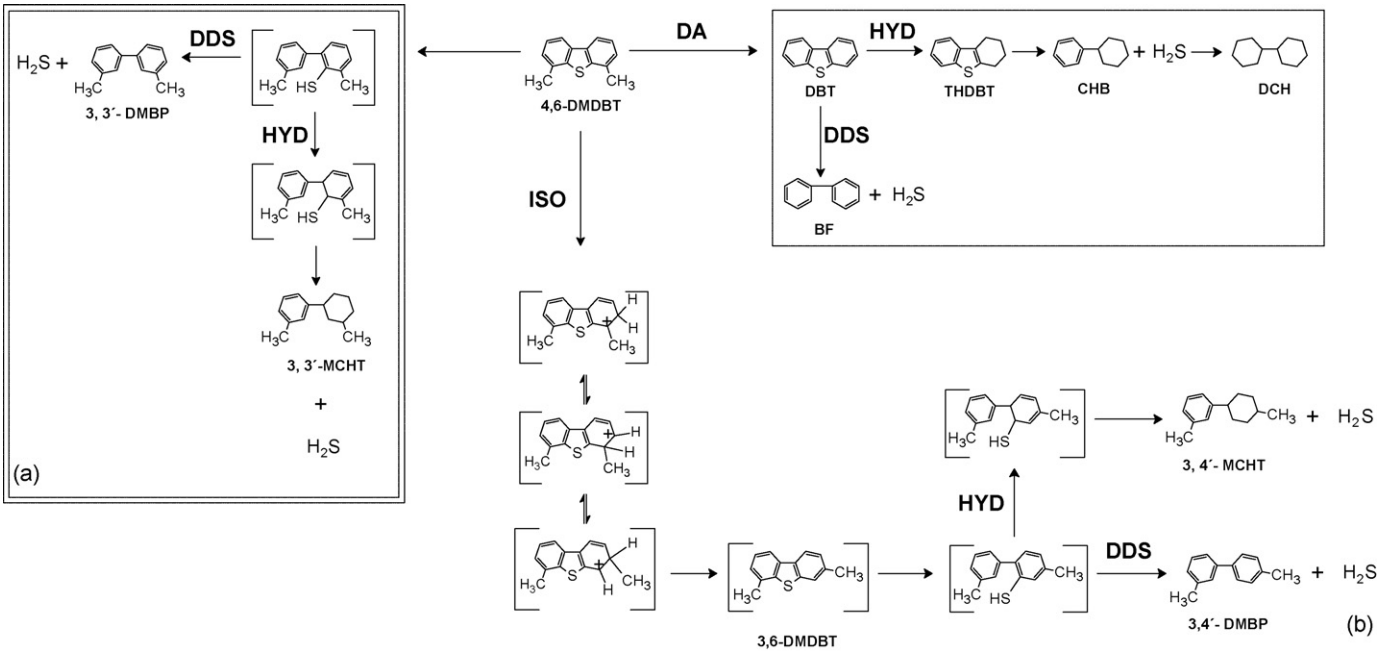

Scheme 1. Reaction scheme for the HDS of 4,6-DMDBT over a reference $CoMoP/Al_2O_3$ sample (a) and CoMo/P/Ti-HMS catalysts (b).

HDS of 4,6-DMDBT on the reference sample, the products obtained in the HDS reaction of 4,6-DMDBT on the SUC-P and SIM-P samples were DBT, BP, THDBT, CHB, DCH, 3,4′-dimethyl-biphenyl (3,4′-DMBP) and 3-(4′-methylcyclohexyl)-toluene (3,4′-MCHT). The HDS of 4,6-DMDBT on SUC-P and SIM-P samples follows two pathways: (i) *via* dealkylation and (ii) *via* isomerization of the methyl-group in the 4,6-DMDBT molecule at the four position migrating to three position in the aromatic ring (Scheme 1(b)). However, one might note that the selectivity at TOS = 0 h is a little different from that obtained at TOS = 10 h. The total 4,6-DMDBT conversion versus time-on-stream is shown in Fig. 6(b). As seen in this figure, both the SIM-P and commercial $CoMoP/Al_2O_3$ samples show greater stability during on-stream conditions than the SUC-P, which showed some activation during the first 3 h of on-stream reaction (1.9%).

The activity results presented above clearly show the following trends: (i) for all synthesized catalysts, the HDS of 4,6-DMDBT proceeds *via* dealkylation and isomerization reaction pathways; (ii) irrespectively of the reactor employed, the SIM catalysts are more active than their counterparts prepared by SUC ones, in good agreement with our previous study [21]; (iii) whichever preparation method is used, P-addition to CoMo/Ti-HMS systems leads to an enhancement of both activity and selectivity toward isomerization route products (see ISO/DA ratio in Tables 3 and 4); (iv) both P-containing catalysts show a larger ISO/DA selectivity ratio when reaction is performed in the fixed-bed reactor; (v) with the

Table 4
Products distribution and the specific reaction rates[a] for HDS of 4,6-DMDBT over SUC-P, SIM-P and reference catalysts

Catalyst	Products distribution (%) at TOS = 0 h (TOS = 10 h)							Selectivity ISO/DA ratio[b]	Selectivity HYD/DDS ratio[c]	4,6-DMDBT conversion (%) at TOS = 0 h (TOS = 10 h)	ν ($mol_{(4,6\text{-}DMDBT)}$ $mol_{(Me)}^{-1}$ s^{-1}) $\times 10^6$ (mol_{Me} = mol Mo + mol Co)
	DBT	THDBT	BF	CHB	DCH	3,4′-DMBP	3,4′-MCHT				
SUC-P	2.9 (2.7)	1.4 (1.9)	6.8 (7.4)	1.7 (1.9)	1.1 (1.3)	31.2 (31.0)	32.6 (33.0)	4.6 (4.3)	1.0 (1.0)	77.7 (79.2)	1.70
SIM-P	1.1 (1.3)	1.0 (1.1)	7.4 (8.2)	1.5 (1.7)	0.9 (1.2)	34.6 (33.6)	36.8 (36.9)	5.9 (5.2)	1.0 (1.0)	83.3 (84.0)	1.81

Catalyst	Products distribution (%) at TOS = 0 h (TOS = 10 h)							Selectivity ISO/DA ratio[b]	Selectivity HYD/DDS ratio[c]	4,6-DMDBT conversion (%) at TOS = 0 h (TOS = 10 h)	ν ($mol_{(4,6\text{-}DMDBT)}$ $mol_{(Me)}^{-1}$ s^{-1}) $\times 10^6$ (mol_{Me} = mol Mo + mol Co)
	DBT	THDBT	BF	CHB	DCH	3,3′-DMBP	3,3′-MCHT				
$CoMoP/Al_2O_3$	–	–	–	–	–	39.9 (38.3)	36.4 (37.9)	–	0.9 (1.0)	76.3 (76.2)	1.1

[a] Reaction was performed in a fixed-bed reactor working under differential conditions (conversion < 15%). The specific reaction rate was calculated according to Eq. (3).
[b] Dealkylation (DA) route products vs. isomerization (ISO) route products: [(DBT + THDBT + BP + CHB + DCH)/(3,4′-DMBP + 3,4′-MCHT)].
[c] Hydrogenation (HYD) route products vs. direct desulfurization (DDS) route products: [(3,4′-MCHT (or 3,3′-MCHT) + THDBT + CHB + DCH)/(3,4′-DMBP (or 3,3′-DMBP) + BP].

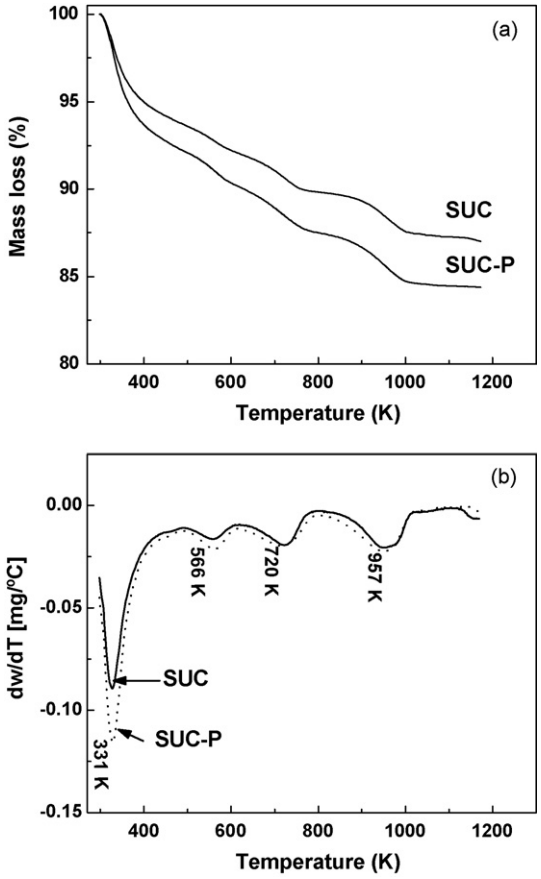

Fig. 7. TGA and DTA profiles of the used SUC and SUC-P.

exception of the P-free SUC catalyst, all synthesized catalysts show a slightly higher activity than the commercial CoMoP/γ-Al_2O_3 catalyst (Tables 3 and 4); (vi) on the commercial catalyst, the 4,6-DMDBT HDS reaction proceeds via HYD and DDS pathways, with the latter being the main reaction route; (vii) whatever the P-loading, catalyst deactivation during on-stream conditions is very low.

3.5. Characterization of the used catalysts

In order to investigate the influence of P on coke formation, the catalysts prepared by successive impregnation were studied by TG-DTA by measuring the weight losses of the coked catalysts upon oxidation in 20% O_2/N_2 mixture. The TG and DTA profiles of the SUC and SUC-P catalysts used are shown in Figs. 7(a) and (b), respectively. The first DTA intense peak, centered at 331 K, cannot be definitively explained, as it lies within the region where the adsorbed water and/or reactant mixture still remaining on the support surface might be desorbed. For both catalysts, the DTA peaks at 566, 720 and 957 K can be ascribed to the burning of coke, being more graphitic at increasing temperature [32]. Considering the P-containing catalyst, the contribution of the volatilization of P_2O_5 phase to the area of peak ca. 957 K could be precluded because the XPS data exclude the presence of this phase on the support surface. It is noteworthy that the area of those three latter peaks is similar for the SUC and SUC-P samples, indicating that the presence of P on the support surface had no influence on coke formation.

In order to investigate the modification undergone by SUC catalyst during on-stream operation, the XPS analysis of the fresh sulfided and used catalysts was performed. Table 5 compiles the binding energy (BE) values and the full width half maximum (FWHM) values of the Mo $3d_{5/2}$ and Co $2p_{3/2}$ (Co–S species) peaks. The Co 2p and Mo 3d core level spectra of the used SUC and SUC-P catalysts are shown in Figs. 8 and 9, respectively. After sulfidation and on-stream reaction, both SUC and SUC-P catalysts show the BE value of the Mo 3d level at 228.9 eV, which is typical of Mo^{4+} in the MoS_2 phase [33]. The formation of the stoichiometric MoS_2 phase could be also deduced from the S/Mo(IV) atomic ratios in range of 2.3–2.7 (see Table 6). Moreover, the full width half maximum (FWHM) values of Mo 3d core level in range 2.2–2.5 indicate that this is the only molybdenum phase formed (Table 5). The used SUC-P catalyst show lower FWHM value than its SUC counterpart (2.2 eV vs. 2.5 eV). Moreover, one might to note that both used samples show larger FWHM values than their fresh sulfided counterparts. The constant line widths of the Si 2p (data not shown here) excludes any charging effects as a possible origin of Mo 3d FWHM variation.

The Co $2p_{3/2}$ core level spectra show two contributions: one at 778.1 eV, indicative of cobalt sulfide [34], and the other at 780.5 eV, indicative of oxide Co^{2+} ions. Considering the BE value of the latter peak, spin-orbit coupling and shake-up satellites, the formation of CoO species is assumed [35,36]. In case of the formation of thermodynamically favoured Co_9S_8 species, the stoichiometric S/Co atomic ratio close to 0.89 could be expected. However, after sulfidation and on-stream reaction both SUC and SUC-P catalysts show the atomic S/Co ratios close to 10 (considering only Co–S species with BE at 778.3 ± 0.2 eV) (Table 5) indicating a large excess of sulfur. Considering the FWHM of the Co $2p_{3/2}$ peak at 778.1 eV (in

Table 5
Binding energies (eV) of core electrons of the fresh sulfided and used catalysts

Catalyst	State	Si 2p	$Mo3d_{5/2}$	FWHM[a] Mo 3d	Co $2p_{3/2}$[b]	FWHM[a] Co $2p_{3/2}$	Co 2p–S 2p
SUC	Sulf.	103.4	228.9	2.3	778.1 (30); 780.4 (70)	3.1	616.7
	Used	103.4	228.9	2.5	778.3 (32); 780.9 (68)	3.5	616.4
SUC-P	Sulf.	103.4	228.8	2.3	778.1 (29); 780.5 (71)	3.2	616.8
	Used	103.4	228.8	2.2	778.4 (31); 780.9 (69)	3.6	616.4

[a] Full width half maximum (FWHM).
[b] Values in parentheses are the relative percentage of each Co $2p_{3/2}$ component.

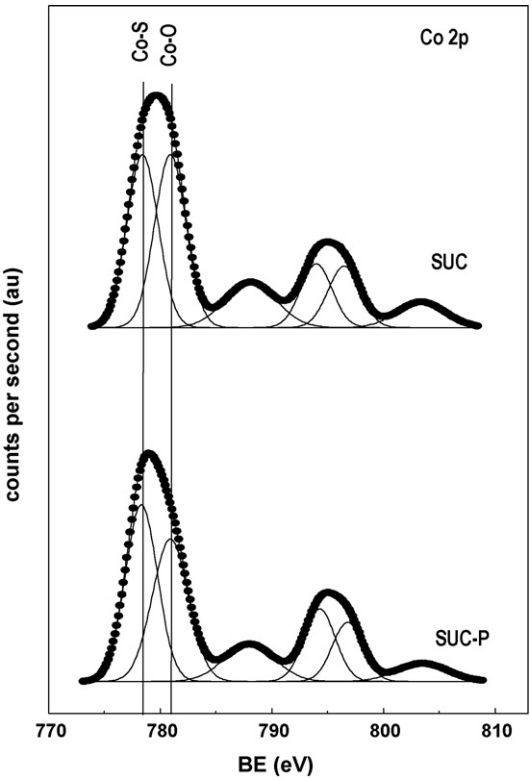

Fig. 8. XPS Co 2p core level spectra of the used SUC and SUC-P samples.

range 3.1–3.5 eV) it can be inferred that only one type of cobalt sulfide species is developed. For the used catalysts, the peak indicative of the cobalt sulfide species is shifted (ca. 0.3 eV) toward higher energy values, but it is still in range where

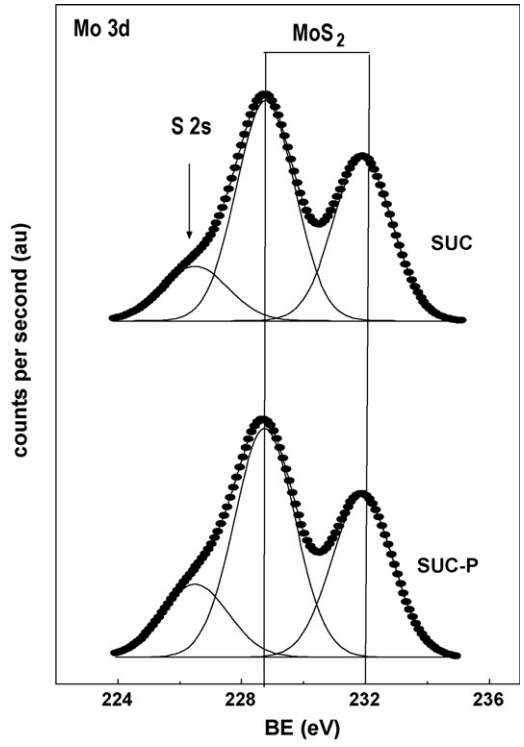

Fig. 9. XPS Mo 3d core level spectra of the used SUC and SUC-P samples.

formation of the Co_9S_8 phase is expected [37]. For the fresh sulfided catalysts, the, the difference in binding energy between the Co $2p_{3/2}$ peak and the S 2p peak (616.8 eV) are larger than the values (615.7–616.2 eV) measured by Alstrup et al. [37] for Co_9S_8 phase and it is close to the value reported for a Co sulfide species interacting with MoS_2 phase [37]. Since the formation of "CoMoS" phase cannot be proved definitively by XPS [38] and the BE of Co $2p_{3/2}$ peak at 780.1 eV is ca. 1 eV lower than those reported for the catalysts containing this phase [39,40], the formation of "CoMoS" phase on the catalysts studied is excluded.

The stability of the active phases during on-stream conditions can be obtained by comparing the Mo/Si, Co/Si and Co(sulf.)/Mo atomic ratios of the freshly sulfided and used catalysts (Table 6). As seen in Table 6, both SUC and SUC-P catalysts show similar Mo surface exposure after sulfidation and on-stream reaction, indicating good stability of its Mo phases. This is confirmed by the similar values of the Co(sulf.)/Mo atomic ratios of the sulfided and used catalysts (Table 6). On the other hand, the comparison of the Co/Si atomic ratio indicate that the presence of P (0.64 wt%) did not influence on the surface exposure of sulfided Co species when SUC impregnation is employed. Considering our previous XPS study on the effect of P-loading into CoMo/HMS catalysts [21], this is a consequence of the very low amount of P incorporated (0.64 wt%), as the incorporation of larger amounts of P (1.5 and 2.0 wt%) leads to an enhancement of the surface exposure of both Mo and Co species. The comparison of S/(Co + Mo) atomic ratios compiled in Table 6, which were calculated taking into account total exposure of Co and Mo ions, might give an idea about the sulfidation degree of the catalysts. The larger S/(Mo + Co) atomic ratio of the fresh sulfided SUC-P catalyst with respect to its P-free counterpart (1.42 vs. 1.37) indicates that the incorporation of P led to an enhancement of the sulfidation degree of Co species (Mo species were fully sulfided).

3.6. Catalyst activity–structure correlation

In this study, synthesized CoMo catalysts were supported on the HMS material stabilized by Ti-incorporation into its framework. The acidic property of the catalyst was modified by P-loading into the Ti-HMS substrate and by using different methods for incorporating the Co and Mo phases (SIM vs. SUC). Catalyst acidity was studied by TPD-NH_3 and DRIFT-NH_3 techniques in order to elucidate factors influenced on the 4,6-DMDBT transformation over those catalysts. The reaction was performed in two different reactors, a batch autoclave and a fixed-bed reactor, in order to evaluate catalyst sensitivity to the intrinsic inhibitors (aromatics and H_2S) present when the reaction is performed in a batch reactor [22].

The superior performance of CoMo catalysts prepared by SIM impregnation could be attributed to the following factors: (i) the larger specific area and the location of active phases on the support surface, as deduced from N_2 sorption measurements (Table 1); (ii) the higher acidity with respect to the catalysts prepared by SUC impregnation, as confirmed by TPD-NH_3 (Table 2) and DRIFT-NH_3 spectroscopy results (Fig. 5); (iii) the increase in the concentration of MoS_2 particles, as derived from

Table 6
Surface exposure of the sulfided and used catalysts as determined by XPS[a]

Catalyst	State	Mo/Si	Co_{total}/Si	(Co–S)/Si	Co 2p(Co–S)/Mo 3d	S/Si	S/(Co–S)	S/Mo	S/(Co_{total} + Mo)
SUC	Sulf.	0.021	0.021	0.006	0.29	0.058	9.1	2.7	1.37
	Used	0.020	0.014	0.005	0.25	0.046	10.3	2.3	1.36
SUC-P	Sulf.	0.022	0.020	0.006	0.27	0.060	10.3	2.7	1.42
	Used	0.020	0.015	0.005	0.25	0.048	10.2	2.4	1.37

[a] Co–S: the sulfided Co species: Co_{total}: sum of the cobalt oxide and sulfide species.

HRTEM (Table 1); (iv) the lower size of the MoS_2 particles formed after sulfidation at 673 K, as determined by HRTEM (Table 1). Moreover, the comparison of the normalized S_{BET} (Table 1) indicates that, contrary to the catalysts prepared by SUC impregnation, for the catalysts prepared by SIM impregnation the reaction mainly occur on the external catalyst surface when the 4,6-DMDBT molecules are adsorbed on the coordinatively unsaturated (CUS) sites of the MoS_2 phase.

Furthermore, it was found that catalyst acidity had a major influence on the reaction pathways in the transformation of 4,6-DMDBT. Thus, for the commercial CoMoP/γ-Al_2O_3 catalyst, the HDS of 4,6-DMDBT reaction proceeds *via* HYD and DDS pathways, whereas the reaction over our synthesized catalysts proceeds via isomerization and dealkylation reaction routes. This is because of their much lower acidity with respect to our siliceous materials and the absence of Brønsted acid sites, as confirmed by TPD-NH_3 and DRIFTS-NH_3. For the synthesized catalysts, Fig. 10 shows the correlation between the yield of the ISO and DA reactions (HDS of 4,6-DMDBT performed in a batch reactor) and the concentration of Brønsted acid sites, as determined by DRIFT-NH_3 (Table 2). It is clear from this figure that ISO is enhanced by an increase in Brønsted acidity, whereas DA follows the opposite trend. Additionally, a correlation between the B/L ratio values and the ISO/DA ratio values of the HDS of 4,6-DMDBT performed in a batch reactor is obtained (Fig. 11). This correlation could also be derived for the reaction performed in the fixed-bed reactor. Although the catalysts tested in the reaction performed in a flow reactor had a similar correlation between acidity and selectivity, it is noteworthy that the ISO/DA ratio for fixed-bed reaction is much larger than those obtained in the batch system (Tables 3 and 4). This difference probably stems from the high adsorption of intermediate products and H_2S on the catalyst active sites when the 4,6-DMDBT HDS reaction is performed in the batch reactor [41]. Additionally, Fig. 11 shows the lineal correlation between total amount of acid sites, as determined by TPD-NH_3 technique, and ISO/DA selectivity ratio. Taking into account that ammonia is not specific probe and can be adsorbed on both Brønsted and Lewis acid sites due to its strong basicity, such correlation suggests that both Brønsted and Lewis acid sites are involved in the reactions of ISO and DA of 4,6-DMDBT molecule.

It is noteworthy that the SIM-P catalyst with the largest proportion of medium strength acid sites shows the largest ISO/DA selectivity ratio among the catalysts studied. By contrast, the SUC catalyst with the largest amount of strong acid sites shows the largest DA. One might therefore conclude that ISO and DA reactions depend on the strength of acid sites also (Fig. 11). The correlation observed in this study between acidity and catalyst activity is in close agreement with other reports [27,42–48]. For example, Isoda et al. [42] reported the ISO of the 4,6-DMDBT in the HDS reaction over physically mixed CoMo/Al_2O_3–Ni/HY catalyst. In this case, the increase of activity was ascribed to the ISO reaction of the alkyl groups in 4,6-DMDBT, minimizing the steric hindrance of the 4,6-DMDBT reactant. Pérot [47], using the physical mixture of NiMo/HY-alumina catalyst, and Bataille et al. [9], using CoMo/zeolite catalyst, also observed an increase in 4,6-DMDBT

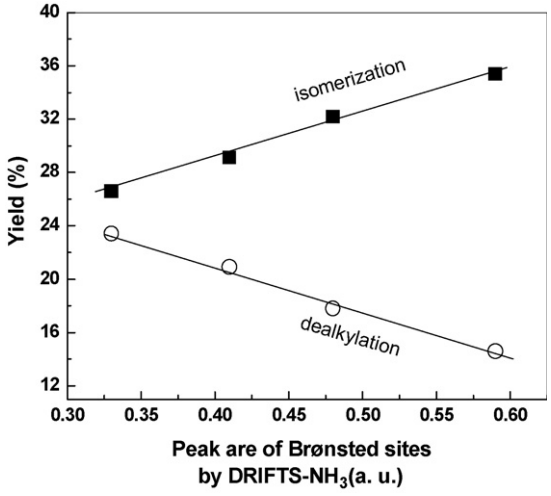

Fig. 10. Correlation between the yield of isomerization and dealkylation products (HDS of 4,6-DMDBT in a batch reactor) and the concentration of Brønsted acid sites.

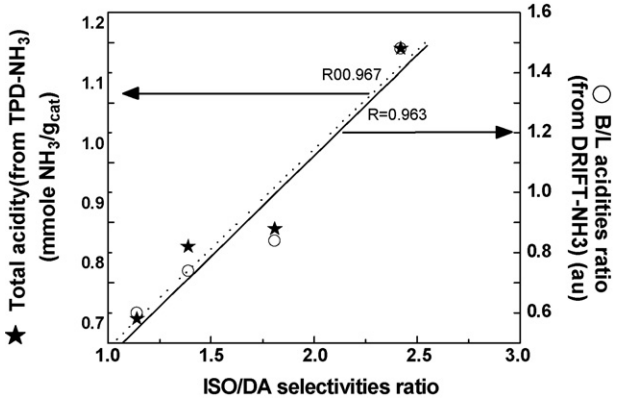

Fig. 11. Influence of the Brønsted-to-Lewis acidities ratio (from DRIFT-NH_3) and the total amount of the acid sites (from TPD-NH_3) on the ISO/DA ratio values (HDS of 4,6-DMDBT; batch reactor).

transformation due to the ISO of one alkyl group in the 4,6-DMDBT molecule. The catalytic activity–acidity correlation observed in this study for the CoMoP/Ti-HMS catalytic systems indicates that the steric hindrance brought about by the alkyl groups in the 4 and 6 positions of DBT might be suppressed by the acid-catalyzed displacement of the alkyl groups and/or disproportionation, in close agreement with our previous study on the P-free CoMo/Ti-HMS systems [22]. Additionally, the acid sites might participate in C–S bond cleavage (DDS route), which is presumably the rate-limiting step in reference to $CoMo/Al_2O_3$ catalysts. The mechanism of C–S bond cleavage assisted by acid sites considers that the acid sites may act as a co-catalyst by providing a proton for easier S-atom removal from the thiophenic ring of the reactant molecule. As a consequence, the consecutive elimination step on S^{2-} ions (acting as basic sites) of the active phase is easier. The proton located on the sulfur can then be transferred to the support in order to regenerate the acid sites. The comparison of the HYD/DDS selectivity ratio (Table 3) with catalyst acidity (Table 2) indicates that an increase in acidity did not enhance the hydrogenation activity of the catalysts. This is contrary to the study by Lecrenay et al. [41] on acidic $CoMo/Al_2O_3$-HY catalysts. Although their catalysts were tested at similar conditions (a batch autoclave, $T = 543–633$ K, $P = 5.0$ MPa), the authors observed that the addition of zeolite with well-controlled acidity provides hydrogenation activity. Consequently, the catalysts were more coke resistant. These authors proposed a mechanism for HYD enhancement over $CoMo/Al_2O_3$-HY catalysts in terms of the H-spillover attacking the reaction intermediate formed on some strong acid sites [41].

In general, the S_{BET} did not correlate with the activity, indicating that support texture was not relevant for the catalytic activity. On the contrary, we found two interesting correlations between average MoS_2 particle size and the density of MoS_2 particles with the catalytic activity (Fig. 12). As seen in Fig. 12(a), the pseudo-first order kinetic rate constants and ISO/DA selectivity ratio increases with an increase of the surface density of MoS_2 particles. On the contrary, the activity and ISO/DA selectivity ratio decreases with increasing MoS_2 particle size (Fig. 12(b)). Thus, it is evident that the catalytic performance of the samples depends on MoS_2 particle size and on the number of MoS_2 particles exposed on the support surface. These observations are consistent with a previous report [49]. Considering the correlation presented in Fig. 11, the decrease in ISO/DA ratio with an increase of MoS_2 particle size is because the acidity decreases when larger MoS_2 particles are formed. From HRTEM, the lower MoS_2 particles are formed on the P-containing samples because those catalysts show a larger Brønsted acidity than P-free counterparts, as demonstrated by DRIFT-NH_3 (Table 2).

By comparison of the correlations presented in Figs. 11 and 12(b), one might to deduce that an increase of the total acidity led to decrease of the MoS_2 particle size. This is expected because both Brønsted and Lewis acid sites might to control the microstructure and the chemical state of the supported Mo and Co oxides [50]. As seen in Fig. 3, the HRTEM images show that the morphological features of the MoS_2 crystallites depend on

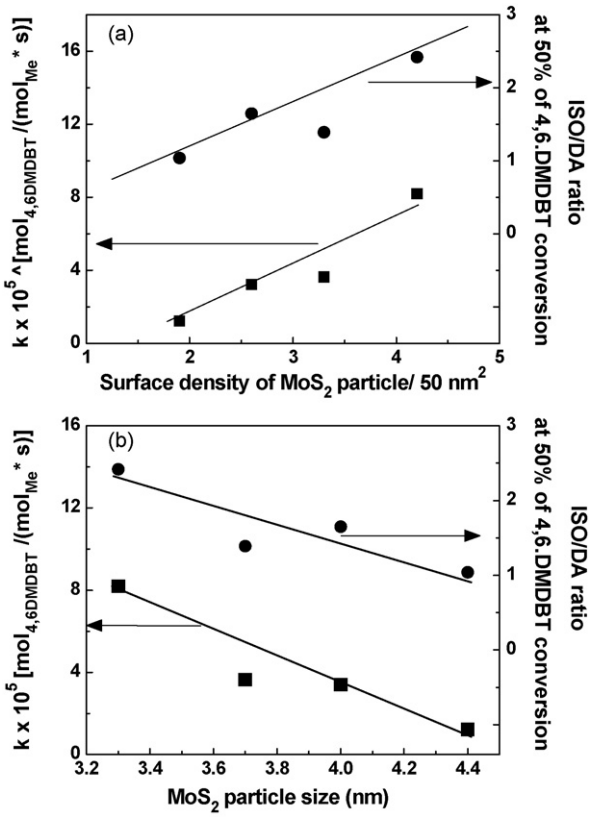

Fig. 12. HDS of 4,6-DMDBT (batch reactor). Influence of the surface density of Mo_2S particles (a) and the MoS_2 particle size (b) on the kinetic rate constants and ISO/DA selectivities ratio. Kinetic rate constants were calculated using Eq. (2) and 4,6-DMDBT conversion reached at reaction time of 6 h.

the presence of P on the support surface. Irrespectively of the catalyst preparation, the statistical HRTEM analysis indicates that after P-addition the particle sizes decrease ca. 0.4 nm (Table 1). Since the MoS_2 shows a layered phase with a hexagonal crystallographic structure, when the particle size decreases a mixed Mo and Co sulfide phase (called ''CoMoS''), in which the Co is located on the MoS_2 edges, could be formed with difficulty [2]. Thus, in good agreement with XPS measurements, the HRTEM study indicate that the ''CoMoS'' phase could be hardly formed on the P-containing catalysts.

The activity-catalysts structure correlation strongly suggests that the absence of the ''Co–Mo–S'' phase formation is not drawback for the high HDS activity of the CoMo/P/Ti-HMS systems. This was observed by us previously [22,26] and it was confirmed recently by Venezia et al. [34] in their study on the monometallic Co catalysts supported on different carriers, who found that the monometallic Co catalyst showed comparable HDS activity as the corresponding binary CoMo sample [34]. In good agreement with our previous study [22,26], the results presented in this study indicate that, besides the active phase dispersion, a specific degree of oxidation/sulfidation of the cobalt species and a high Co/Mo ratio might account for a high activity of the CoMo/P/Ti-HMS systems with respect to a reference $CoMoP/Al_2O_3$ catalyst. The hydrogen activation on the cobalt oxide species [36] and/or the activation of 4,6-DMDBT molecules on the S-vacancies in the Co_9S_8 phase

[51,52] might also explain our results. Unfortunately, our data do not allow drawing definitive conclusions about it.

To conclude, this study shows that the two impregnation methods employed in the preparation of the catalysts and the presence of P have multiple and complex effects on the morphologic, structural, and acid properties of the supported Co and Mo species. The most optimized catalyst was prepared by SIM impregnation of the P/Ti-HMS material. For this catalyst, the ISO route of the HDS of 4,6-DMDBT reaction was enhanced due to its best morphology and acid properties among the catalysts studied. However, it must be stressed that the commercial utility of the CoMo/P/Ti-HMS catalyst cannot be assessed until a comparison is made with the latest generation of HDS bulk-type catalysts (e.g. NEBULA) and long-term pilot plant experiments have been performed.

4. Conclusions

(i) The HDS of 4,6-DMDBT over supported CoMo catalysts prepared by SUC and SIM impregnation proceeds *via* DA and principally *via* isomerization pathways, both followed by hydrogenation and DDS pathways, while the reaction over the commercial CoMoP/γ-Al_2O_3 sample proceeds only *via* hydrogenation and mainly *via* desulphurization reaction pathways.

(ii) ISO and DA reactions depend strongly on the presence of Brønsted acid sites, total acidity and the strength of acid sites.

(iii) The enhancement of activity and ISO observed with the catalyst prepared by SIM impregnation and modified with P was related to the cumulative effects of the lower size of Mo_2S particles and their higher surface density.

Acknowledgements

The authors thank E. Betancourt, E. Flores and Dr. M. Peña for their technical assistance. T.A.Z. wishes to express his gratitude to CONACyT, DGEP- and DGAPA-UNAM, Mexico, for financial support. The Spanish Ministry of Science and Technology is also acknowledged for funding the ENE2004-07345-C03-01/ALT project.

References

[1] H. EP Directive 2003/17/EC, Office Journal of the European Union L76, 46 (2003) 10.
[2] H. Topsøe, B.S. Clausen, F.E. Massoth, Hydrotreating Catalysts: Science and Technology, Springer, Berlin, 1996, p. 310.
[3] D.D. Whitehurst, T. Isoda, I. Mochida, Adv. Catal. 42 (1998) 345.
[4] I.V. Babich, J.A. Moulijn, Fuel 82 (2003) 607.
[5] R. Shafi, G.J. Hutchings, Catal. Today 59 (3/4) (2000) 423.
[6] F.L. Plantenga, R.G. Leliveld, Appl. Catal. A 248 (2003) 248.
[7] W.R.A.M. Robinson, J.A.R. van Veen, V.H.J. de Beer, R.A. van Santen, Fuel Proc. Technol. 61 (1999) 89.
[8] W.R.A.M. Robinson, J.A.R. van Veen, V.H.J. de Beer, R.A. van Santen, Fuel Proc. Technol. 61 (1999) 103.
[9] F. Bataille, J.L. Lemberton, G. Pérot, P. Leyrit, T. Cseri, N. Marchal, S. Kasztelan, Appl. Catal. A 220 (2001) 191.
[10] M.V. Landau, D. Berger, M. Herskowitz, J. Catal. 158 (1996) 236.
[11] T. Isoda, S. Nagao, X. Ma, Y. Korai, I. Mochida, Energy Fuels 10 (1996) 1078.
[12] P. Michaud, J.L. Lemberton, G. Perot, Appl. Catal. A 169 (1998) 343.
[13] E. Lecrenay, K. Sakanishi, T. Nagamatsu, I. Mochida, T. Suzuka, Appl. Catal. B 18 (1998) 325.
[14] C. Kwak, M.Y. Kim, K. Choi, S.H. Moon, Appl. Catal. A 185 (1999) 19.
[15] J.M. Manoli, P. Da Costa, M. Brun, M. Vrinat, F. Maugé, C. Potvin, J. Catal. 221 (2004) 365.
[16] P.J. Mangnus, J.A.R. van Veen, S. Eijbouts, V.H.J. de Beer, J.A. Moulijn, Appl. Catal. 61 (1990) 99.
[17] P.J. Mangnus, A.D. van Langeveld, V.H.J. de Beer, J.A. Moulijn, Appl. Catal. 68 (1991) 161.
[18] H. Kraus, R. Prins, J. Catal. 164 (1996), 251, 260.
[19] J.C. Edwards, P.D. Ellis, Langmuir 7 (1991) 2117.
[20] M. Breysse, B.A. Benett, D. Chadwick, M. Vrinat, Bull. Soc. Chim. Belg. 90 (1981) 1271.
[21] R. Nava, J. Morales, G. Alonso, C. Ornelas, B. Pawelec, J.L.G. Fierro, Appl. Catal. A 321 (2007) 58.
[22] T.A. Zepeda, B. Pawelec, J.L.G. Fierro, T. Halachev, Appl. Catal. B 71 (2007) 223.
[23] S. Gotier, A. Tuel, Zeolites 15 (1995) 601.
[24] T.A. Zepeda, J.L.G. Fierro, B. Pawelec, R. Nava, T. Klimova, G.A. Fuentes, T. Halachev, Chem. Mater. 17 (2005) 4062.
[25] C. Song, Catal. Today 86 (2003) 211.
[26] L. Vradman, M.V. Landau, D. Kantorovich, Y. Koltypin, A. Gedanken, Micropor. Mesopor. Mater. 70 (2005) 307.
[27] T.A. Zepeda, B. Pawelec, J.L.G. Fierro, T. Halachev, J. Catal. 242 (2006) 254.
[28] M.A. Centeno, I. Carrizosa, J.A. Odriozola, Appl. Catal. B 29 (2001) 307.
[29] L.V.C. Rees, G. Onyestyák, Micropor. Mesopor. Mater. 28 (1999) 293.
[30] W. Zhang, P.G. Smirniotis, Appl. Catal. A 168 (1998) 113.
[31] NIST Reference Database N° 69, http://webbook.nist.gov/chemistry/.
[32] B. Pawelec, V. La Parola, S. Thomas, J.L.G. Fierro, J. Mol. Catal. A: Chem. 253 (2006) 30.
[33] D. Briggs, M.P. Seah (Eds.), Practical Surface Analysis. Auger and X-ray Photoelectron Spectroscopy, Wiley, New York, 1990.
[34] A.M. Venezia, V. La Parola, G. Deganello, D. Cauzzi, G. Leonardi, G. Predieri, Appl. Catal. A: Gen. 229 (2002) 261.
[35] Y. Okamoto, T. Imanaka, S. Teranishi, J. Catal. 65 (1980) 448.
[36] A.M. Venezia, R. Murania, G. Pantaleo, G. Deganello, J. Mol. Catal. A: Chem. 271 (2007) 238.
[37] I. Alstrup, I. Chorkendorff, R. Candia, B.S. Clausen, H. Topsøe, J. Catal. 77 (1982) 397.
[38] A.M. de Jong, V.H.J. de Beer, J.A. Rob van Veen, J.W. Niemantsverdriet, J. Phys. Chem. 100 (1996) 17722.
[39] Y. Okamoto, T. Kubota, Catal. Today 86 (2003) 31.
[40] M.A. Cortés-Jácome, J. Escobar, C. Angeles Chávez, E. López-Salinas, E. Romero, G. Ferrat, J.A. Toledo-Antonio, Catal. Today 130 (2008) 56.
[41] E. Lecrenay, K. Sakanishi, I. Mochida, Catal. Today 39 (1997) 13.
[42] T. Isoda, S. Nagao, Y. Korai, I. Mochida, Am. Chem. Soc. Prepr. Div. Petrol. Chem. 41 (1996) 563.
[43] T. Kabe, A. Ishihara, H. Tajima, Ind. Eng. Chem. Res. 31 (1992) 218.
[44] A. Ishihara, H. Tajima, T. Kabe, Chem. Lett. (1992) 669.
[45] D.H. Kilanowski, H. Teeuwen, V.H.J. De Beer, B.C. Gates, G.C.A. Schuit, H. Kwart, J. Catal. 55 (1978) 129.
[46] M.V. Landau, Catal. Today 36 (1997) 393.
[47] G. Pérot, Catal. Today 86 (2003) 111.
[48] F. Richard, T. Boita, G. Pérot, Appl. Catal. A 320 (2007) 69.
[49] T.A. Zepeda, B. Pawelec, A. Olivas, J.L.G. Fierro, Mater. Res. Innov. 11 (1) (2007) 54.
[50] R.G. Leliveld, T.G. Ros, A.J. van Dillen, J.W. Geus, D.C. Koningsberger, J. Catal. 185 (1999) 513.
[51] R.G. Leliveld, A.J. van Dillen, J.W. Geus, D.C. Koningsberger, J. Catal. 175 (1998) 108.
[52] B.R.G. Leliveld, J.A.J. van Dillen, J.W. Geus, D.C. Koningsberger, M. de Boer, J. Phys. Chem. 101 (1997) 1116.